

High spin polarization in epitaxial Fe₄N thin films using Cr and Ag as buffer layers

Cite as: Appl. Phys. Lett. **112**, 162407 (2018); <https://doi.org/10.1063/1.5023698>

Submitted: 26 January 2018 . Accepted: 04 April 2018 . Published Online: 18 April 2018

Hongshi Li, Xuan Li, Dongrin Kim, Gejian Zhao, Delin Zhang, Zhitao Diao, Tingyong Chen , and Jian-Ping Wang



View Online



Export Citation



CrossMark

ARTICLES YOU MAY BE INTERESTED IN

[Electric field modulated ferromagnetism in ZnO films deposited at room temperature](#)

Applied Physics Letters **112**, 162408 (2018); <https://doi.org/10.1063/1.5022597>

[Invisible magnetic sensors](#)

Applied Physics Letters **112**, 162406 (2018); <https://doi.org/10.1063/1.5023565>

[Enhancement of tunneling magnetoresistance by inserting a diffusion barrier in L1₀-FePd perpendicular magnetic tunnel junctions](#)

Applied Physics Letters **112**, 152401 (2018); <https://doi.org/10.1063/1.5019193>

Applied Physics Reviews
Now accepting original research

2017 Journal
Impact Factor:
12.894

AIP
Publishing

High spin polarization in epitaxial Fe₄N thin films using Cr and Ag as buffer layers

Hongshi Li,¹ Xuan Li,² Dongrin Kim,³ Gejian Zhao,³ Delin Zhang,² Zhitao Diao,⁴ Tingyong Chen,³ and Jian-Ping Wang^{1,2,a)}

¹Department of Chemical Engineering and Materials Science, University of Minnesota, Minneapolis, Minnesota 55455, USA

²Department of Electrical and Computer Engineering, University of Minnesota, Minneapolis, Minnesota 55455, USA

³Department of Physics, Arizona State University, Tempe, Arizona 85287, USA

⁴Western Digital Corporation, San Jose, California 95119, USA

(Received 26 January 2018; accepted 4 April 2018; published online 18 April 2018)

Fe₄N thin films with (001) texture were prepared by reactive sputtering on MgO substrates, utilizing either a Cr or Ag buffer layer to facilitate the epitaxial growth. X-ray diffraction, atomic force microscopy, and vibrating sample magnetometry measurements show that the Fe₄N thin film grown on the Ag buffer layer is superior to that grown on the Cr buffer layer. The point contact Andreev reflection measurement was then conducted, and the spin polarizations were determined to be 61.1% and 81.3% for Fe₄N thin films with Cr and Ag buffer layers, respectively. The 81.3% spin polarization is significantly higher than the ratio reported previously for Fe₄N and is comparable with that of state-of-the-art Heusler alloys. This result is in agreement with the theoretical prediction on the discrepancy between the two differently defined spin polarizations for Fe₄N. Moreover, our study indicates that an optimized growth process for Fe₄N thin films is crucial for achieving a high spin polarization and that true half-metallicity could potentially be realized with Fe₄N. The high spin polarization of Fe₄N combined with its low fabrication temperature and simple composition makes Fe₄N a competitive candidate to be a half-metallic ferromagnet in spintronic devices. *Published by AIP Publishing.* <https://doi.org/10.1063/1.5023698>

Half-metallic ferromagnets (HMFMs) are of scientific interest and technological importance because there is only one spin band available at the Fermi level, which gives rise to a current with full spin polarization (SP).¹ The efficiency of spintronic devices such as magnetic tunnel junctions (MTJ), giant magnetoresistance devices, and spin-transfer torque devices will be greatly enhanced if their ferromagnetic layers are replaced with HMFMs.^{2–5} Previously, CrO₂ has been the only HFM that has demonstrated 98% spin polarization (SP ratio),^{6,7} but it has a low T_c and instability at room temperature. In addition, Heusler alloys and LaSrMnO have also been proposed to be half-metallic, but their spin polarization is often less than 85%.^{8–11} The difficulty in their fabrication and their complicated composition also limit their application.

Fe₄N has been extensively studied due to its high SP ratio, high Curie temperature, and low coercivity.^{12–17} Unlike conventional ferromagnetic materials, Fe₄N has a negative spin polarization ratio.¹⁸ As a result, negative anisotropic magnetoresistance and MTJ devices with negative magnetoresistance ratios have been demonstrated.^{19,20} Tunable perpendicular magnetic anisotropy under an electric field is predicted, granting Fe₄N even more potential for applications in spintronics.^{21,22} Cubic to tetragonal structural transformation in the Fe₄N lattice at low temperature and concurrent change in transport behaviors have been observed.^{23,24} Alternative tetra-3d metal nitrides, such as Co₄N and Ni₃FeN, which share key features with Fe₄N, have

been actively explored.^{25–27} Particularly, Fe₄N has been theoretically predicted by Kokado *et al.* to be a HFM with a transport SP ratio close to 100%.¹² Compared with Heusler alloys, the most extensively studied HFM hitherto, Fe₄N shows a major advantage in terms of fabrication. While the 500–700 °C^{28–32} annealing temperatures required to form an ordered structure in Heusler alloys render major obstacles for fabrication of spintronic devices, Fe₄N can be prepared at a lower temperature in the range of 150–400 °C.^{13–17,33} The low preparation temperature of Fe₄N combined with its simple composition and crystalline structure grants Fe₄N additional advantages when compared to Heusler alloys for use as a ferromagnetic electrode.

However, despite the predicted half-metallicity, the previous point contact Andreev reflection (PCAR) measurement of Fe₄N thin films shows an SP ratio of 59%.³⁴ The 59% SP ratio is comparable to the ratio of CoFeB estimated by the same method³⁵ but is significantly less than the theoretically predicted value and the ratio of state-of-the-art Heusler alloys.^{8,9} The large discrepancy between theoretically predicted and experimentally determined SP ratios calls into question the potential of Fe₄N as a HFM. In this work, we will show that a higher SP ratio could be achieved in Fe₄N. Fe₄N thin films with (001) texture were sputtered onto single crystal MgO (001) substrates with either Cr or Ag as a buffer layer. The films were characterized by X-ray diffraction (XRD), atomic force microscopy (AFM), and vibrating sample magnetometry (VSM). The PCAR measurement was then conducted to determine the SP ratio. Our work demonstrates an 81.3% SP ratio in the Fe₄N film and indicates that

^{a)}Electronic mail: jpwang@umn.edu

true half-metallicity could potentially be achieved with Fe_4N .

Fe_4N films with stack structures $\text{MgO}/\text{Cr}/\text{Fe}_4\text{N}$ and $\text{MgO}/\text{Fe}/\text{Ag}/\text{Fe}_4\text{N}$ were prepared using a multi-facing-target sputtering system. The facing-target sputtering cathode design of the sputtering system avoids direct contact between the plasma and the substrate, thus reducing the energy involved during the deposition process.^{36,37} The single crystal MgO (001) substrates were overlaid with either Cr or Fe/Ag buffer layers to facilitate epitaxial growth. The Fe_4N layer was deposited at $240 \pm 40^\circ\text{C}$ by reactive sputtering, where Ar gas was mixed with N_2 gas with an optimized partial pressure.³⁸ Since the substrate heating was not *in situ*, 60 nm Fe_4N was grown in two steps to maintain the growth temperature. In each step, the substrates were heated in the load-lock and then transferred to the main chamber to deposit a 30 nm Fe_4N layer. Finally, the film stacks were annealed at 350°C for 30 min to further improve crystallinity. Films with stack structures $\text{MgO}-\text{Cr}(50)\text{Fe}_4\text{N}(60)$ and $\text{MgO}-\text{Fe}(3)\text{Ag}(30)\text{Fe}_4\text{N}(60)$ were used for AFM and PCAR measurements, while films with stack structures $\text{MgO}-\text{Cr}(20)\text{Fe}_4\text{N}(60)\text{Ag}(5)\text{Cr}(10)$ and $\text{MgO}-\text{Fe}(2)\text{Ag}(20)\text{Fe}_4\text{N}(60)\text{Ag}(5)\text{Cr}(10)$ were used for VSM and XRD measurements. The numbers in parentheses are the nominal thickness in nanometers. The Fe buffer layer thickness was minimized to reduce any potential interference the Fe layer might have had on the characterization of the Fe_4N film. The qualities of the buffer layers were verified despite some variation in thickness. The $\text{Ag}(5)\text{Cr}(10)$ capping layers were deposited to provide additional protection and are not expected to interfere with the measurements.

Structural characterization was carried out by X-ray diffraction using a Panalytical X'Pert Pro diffractometer with Cu K-alpha radiation. In contrast to the single phase Fe_4N achieved in the 17 nm Fe_4N films in our previous experiments,³⁸ a strong Fe_4N (002) peak and a weak Fe_3N (001) peak were observed in the XRD spectrum for the 60 nm Fe_4N films grown on either a Cr or Ag buffer layer, as shown in Fig. 1(a). Since the substrate heating was *ex situ*, the Fe_3N phase might have resulted from the drop in substrate temperature during the relatively long time of deposition. Given a certain Ar and N_2 mixture ratio, a lower growth temperature tends to foster the Fe_3N phase.¹³ The lattice constant of Fe_4N is calculated to be 3.806 \AA and 3.808 \AA for Cr and Ag buffered Fe_4N films, respectively, which are close to the theoretical value of 3.795 \AA , despite lattice mismatches with the buffer layers. To determine the texture of the Fe_4N films, rocking curve measurements were conducted. The FWHM values of 1.80° and 1.12° were measured for Cr and Ag buffered Fe_4N films, respectively, as seen in Fig. 1(b). Therefore, a better texture is achieved for the Fe_4N film grown on a Ag buffer layer, although neither of the films has a pure Fe_4N phase.

Surface topographies of 60 nm Fe_4N films taken with a Bruker atomic force microscope in the tapping mode are shown in Fig. 2. The Fe_4N film with the Cr buffer layer shows a much larger grain size than that with the Ag buffer layer. Correspondingly, the RMS roughness of the Fe_4N films is determined to be 3.0 nm and 0.37 nm for Cr and Ag buffered films, respectively, which exhibits almost an order of magnitude difference. This indicates that Fe_4N might

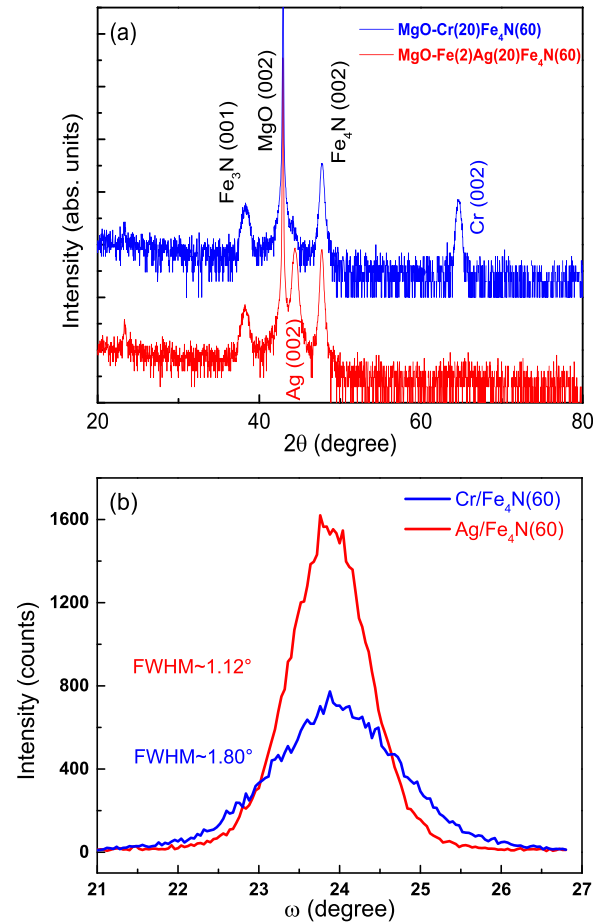


FIG. 1. (a) θ - 2θ XRD scans of the Fe_4N films grown on Cr and Ag buffer layers. (b) Rocking curve measurement of Fe_4N (002) peaks.

have a lower interfacial energy and a better adhesion with Ag than with the Cr buffer layer.

The in-plane vibrating sample magnetometer (VSM) measurement with the field applied along the [100] direction was conducted using a Physical Property Measurement System (PPMS) in a temperature range of 5–360 K. M-H loops at room temperature are shown in Figs. 3(a) and 3(b). The sharp magnetization switching and high M_r/M_s ratios indicate well-ordered epitaxial growth for both films. However, a stronger field is needed to fully saturate the magnetization. This might result from the presence of the Fe_3N phase whose coercivity is reported to be higher than 500 Oe at room temperature.³⁹ Figures 3(c) and 3(d) depict the temperature dependence of the saturation magnetization and the coercivity of the Fe_4N films with Cr and Ag buffer layers, respectively. The contribution from the Fe buffer layer to magnetization has been subtracted for the Ag buffered sample. As the temperature increases from 5 K to 360 K, saturation magnetization decreases from 1285 emu/cc to 1052 emu/cc for the Cr buffered sample and from about 1314 emu/cc to 1118 emu/cc for the Ag buffered sample. Meanwhile, coercivity decreases from 130 Oe to 63 Oe for the Cr buffered sample and from 117 Oe to 46 Oe for the Ag buffered sample. By using Bloch's spin wave theory to fit the data,^{14,40} the saturation magnetization at 0 K is determined to be 1242 emu/cc and 1296 emu/cc for the Cr and Ag buffered samples, respectively. The lower coercivity in the

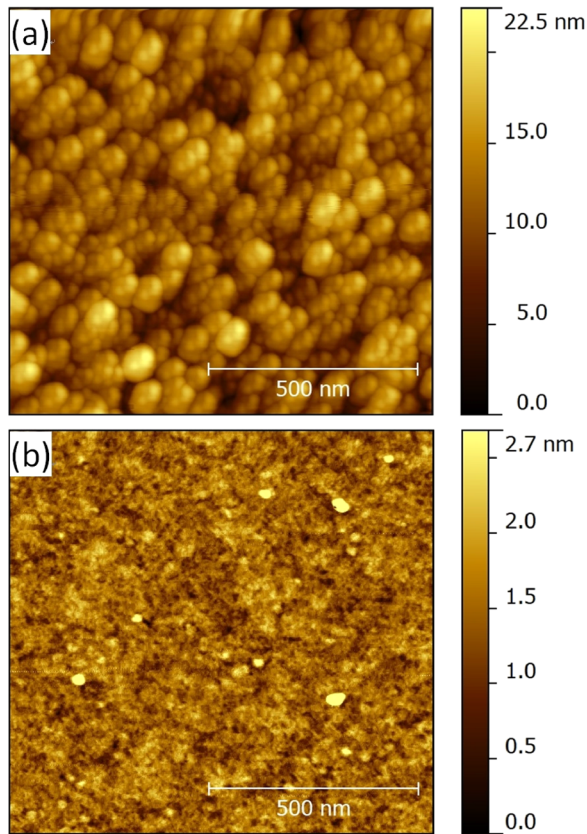


FIG. 2. AFM images of 60 nm Fe_4N films. The RMS roughness is 3.0 nm for (a) the Cr buffered sample and 0.37 nm for (b) the Ag buffered sample.

Ag buffered sample is in accordance with the smaller roughness shown by the AFM measurement described above.⁴¹ Its higher M_s is also in agreement with the better film qualities determined from previous characterization studies.

The SP ratio of the Fe_4N thin films was explored with PCAR testing.^{10,42} The measurement was conducted at 4.2 K by gently pushing a superconducting Pb probe through the

native oxide to form contact with the Fe_4N film.⁸ Andreev reflection (AR) spectra which depict normalized conductance $G(V)/G_n$ versus bias voltage V were then collected, where G_n is the normal state conductance without Andreev reflection. Since the characterized SP ratio is dependent on interfacial scattering (Z) between the Pb probe and the Fe_4N film, the point contacts were repeated numerous times, each generating an AR spectrum exemplified in Fig. 4. The AR spectra were then individually fitted to the modified Blonder-Tinkham-Klapwijk (BTK) model.⁴³ The fitting parameters include the SP ratio, P , the interfacial scattering strength factor, Z , and the extra resistance, r_E .⁴³ The fitted SP ratio is plotted against the Z factor in Fig. 5 and fitted with a polynomial curve to find the intrinsic SP ratio of Fe_4N . The intrinsic SP ratio was determined to be $61.1 \pm 3\%$ and $81.3 \pm 1\%$ for Fe_4N grown on the Cr and Ag buffer layers, respectively. Due to the spin dephasing effect in ferromagnets, the PCAR measurement is only sensitive to the material less than a few nanometers away from the probe. Therefore, the presence of an Fe buffer layer will not affect the measurement. As a control measurement, an Fe (001) sample was also characterized with the same measurement, and its SP ratio value was in agreement with that from a previous report.³⁴

The large contrast between the SP ratios of Fe_4N grown on the Cr and Ag buffer layers could be understood as follows: All previous XRD, AFM, and VSM measurements indicate that the Fe_4N film grown on a Ag buffer layer has better crystalline and surface/interface qualities than that grown on a Cr buffer layer. The results suggest that the SP ratio of Fe_4N thin films might be very sensitive to their growth processes and that optimization of Fe_4N film growth conditions is crucial. In our previous work, the Fe_4N film with (111) texture was prepared on thermally oxidized Si substrates, where Ta/Ru composite buffer layers were adopted to foster the texture.⁴⁴ Since thermal oxidized Si is amorphous, the growth was not epitaxial. The SP ratio of the

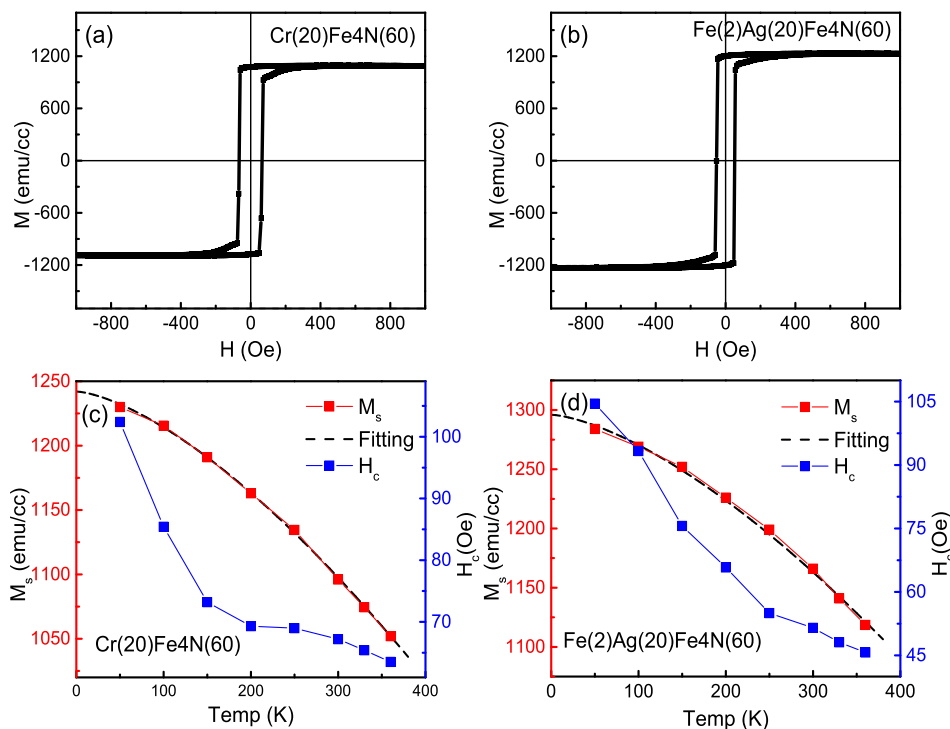


FIG. 3. Magnetic properties of Fe_4N films. Hysteresis loops at room temperature for the Fe_4N films grown on (a) Cr and (b) Ag buffer layers are shown. The temperature dependence of saturation magnetization and coercivity of (c) Cr and (d) Ag buffered Fe_4N films is shown.

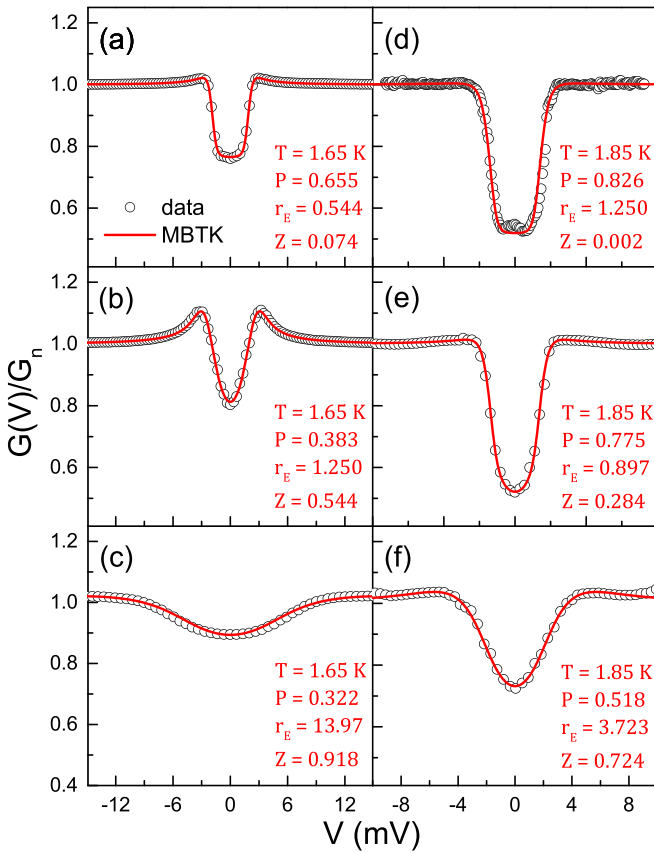


FIG. 4. Representative Andreev spectra of Fe_4N thin films using (a)–(c) Cr and (d)–(f) Ag as buffer layers. Open circles are experimental data, while solid curves are the best fit to the modified BTK model with fitting parameters listed in the insets, with T the experimental temperature, P the spin polarization, r_E the extra resistance, and Z the interfacial scattering factor. The superconducting tip is lead with a gap value of 1.31 meV.

(111) textured Fe_4N film was determined by the PCAR measurement to be only 50%. Although more systematic research is needed before any solid conclusion can be drawn about the influence of the crystalline orientation, this result further indicates the importance of an optimized growth process for achieving a high SP ratio in Fe_4N . The 81.3% SP ratio achieved here is significantly higher than the highest SP ratio reported on Fe_4N previously, which is 59%,³⁴ and is comparable or even higher than that of state-of-the-art Heusler alloys.^{8–10} Most importantly, although the SP ratio was improved drastically from 61.1% to 81.3% by switching the buffer layer from Cr to Ag, the Fe_4N film with a Ag buffer layer is by no means perfect. In other words, there might still be room for improvement in the SP ratio, and true half-metallicity could potentially be achieved with Fe_4N .

Moreover, it should be noted that there are two distinct definitions for the SP ratio,^{10,12} whose difference has often been neglected. One of the definitions is based on the density of states (DOS) of spin up and spin down electrons at the Fermi level, which we refer to as the DOS SP ratio. The other definition is based on the spin up and spin down electrons' contribution to transport, where the DOSs are weighted by the Fermi velocities, which we refer to as the transport SP ratio. Despite the fact that Fe_4N is known as a potential half-metallic ferromagnet, none of the simulations of the spin resolved electronic structure of Fe_4N have so far showed a

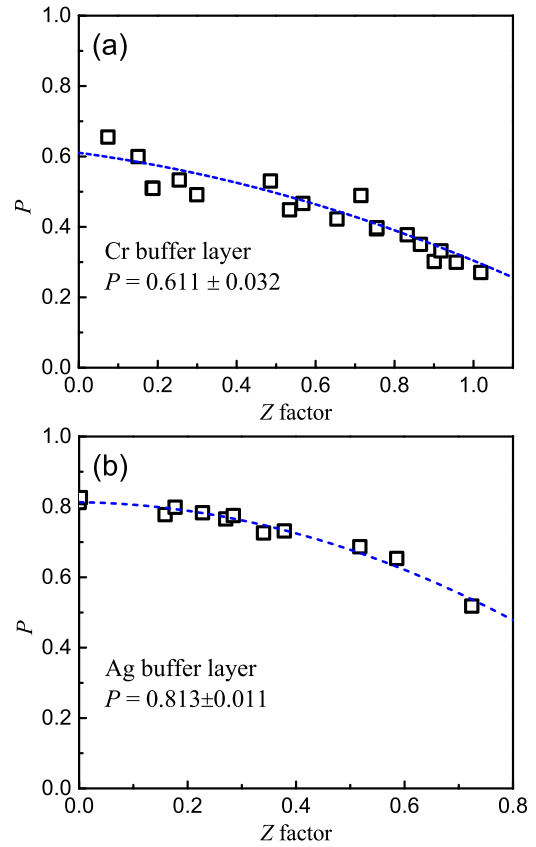


FIG. 5. Spin polarization of Fe_4N films with buffer layers (a) Cr and (b) Ag as a function of interfacial scattering factor Z .

high DOS SP ratio,^{12,45–48} including the work of Kokado *et al.*¹² which reports a DOS SP ratio of only 60%. However, the same work indicates that when the Fermi velocities of electrons in different bands are taken into consideration, the transport SP ratio in Fe_4N could be close to 100%. In the PCAR experiment, the transport SP ratio rather than the DOS SP ratio is characterized.¹⁰ Thus, the 81.3% transport SP ratio we measured in Fe_4N , though still less than 100%, is indeed higher than the 60% DOS SP ratio predicted, which largely confirms the current theoretical prediction.

In conclusion, Fe_4N thin films with a (001) texture were developed on single crystal MgO (001) substrates on either Cr or Ag buffer layers. The transport SP ratios were determined by the PCAR measurement to be 61.1% and 81.3% for Fe_4N (001) films grown on the Cr and Ag buffer layers, respectively. The 81.3% SP ratio is significantly higher than the 59% ratio in the previous report on Fe_4N and is comparable to the SP ratio of state-of-the-art Heusler alloys. This result is in agreement with the theoretical prediction on the discrepancy between the two differently defined spin polarizations in Fe_4N . The high transport SP ratio of Fe_4N along with its simple composition and low fabrication temperature makes Fe_4N a potential candidate to be a half-metallic ferromagnetic electrode in spintronic devices. Moreover, the large contrast in SP ratios of Fe_4N thin films with different buffer layers combined with the XRD, AFM, and VSM analyses also suggests that the SP ratio of Fe_4N is very sensitive to its growth processes and the qualities of the films. Given the high SP ratio obtained in our non-state-of-the-art sample, a

full spin polarization, or true half-metallicity, could potentially be achieved with Fe₄N.

The authors thank the useful discussion with Dr. Qunwen Leng. This work was supported by Western Digital Corporation. Part of this work was carried out at the Characterization Facility, University of Minnesota, a member of the NSF-funded Materials Research Facilities Network (www.mrfln.org) via the NSF MRSEC Program under Award No. DMR-0819885. The PCAR testing was supported as part of SHINES, an EFRC center funded by the U. S. Department of Energy, Office of Science, Basic Energy Science, under Award No. SC0012670.

- ¹R. A. de Groot and F. M. Mueller, *Phys. Rev. Lett.* **50**, 2024 (1983).
- ²M. Julliere, *Phys. Lett. A* **54**, 225 (1975).
- ³Y. Du, T. Furubayashi, T. T. Sasaki, Y. Sakuraba, Y. K. Takahashi, and K. Hono, *Appl. Phys. Lett.* **107**, 112405 (2015).
- ⁴Y. Sakuraba, K. Izumi, T. Iwase, S. Bosu, K. Saito, K. Takanashi, Y. Miura, K. Futatsukawa, K. Abe, and M. Shirai, *Phys. Rev. B* **82**, 094444 (2010).
- ⁵S. Tsunegi, Y. Sakuraba, M. Oogane, K. Takanashi, and Y. Ando, *Appl. Phys. Lett.* **93**, 112506 (2008).
- ⁶Y. Ji, G. J. Strijkers, F. Y. Yang, C. L. Chien, J. M. Byers, A. Anguelouch, G. Xiao, and A. Gupta, *Phys. Rev. Lett.* **86**, 5585 (2001).
- ⁷A. Anguelouch, A. Gupta, G. Xiao, D. Abraham, Y. Ji, S. Ingvarsson, and C. Chien, *Phys. Rev. B* **64**, 180408(R) (2001).
- ⁸M. Vahidi, J. A. Gifford, M. Huang, C. Youngbull, T. Y. Chen, and N. Newman, *APL Mater.* **2**, 046108 (2014).
- ⁹B. S. D. C. S. Varaprasad, A. Srinivasan, Y. K. Takahashi, M. Hayashi, A. Rajanikanth, and K. Hono, *Acta Mater.* **60**, 6257 (2012).
- ¹⁰R. J. Soulen, J. M. Byers, M. S. Osofsky, B. Nadgorny, T. Ambrose, S. F. Cheng, P. R. Broussard, C. T. Tanaka, J. Nowak, J. S. Moodera, A. Barry, and J. M. D. Coey, *Science* **282**, 85 (1998).
- ¹¹Y. Ji, C. L. Chien, Y. Tomioka, Y. Tomioka, Y. Tokura, Y. Tokura, and Y. Tokura, *Phys. Rev. B* **66**, 012410 (2002).
- ¹²S. Kokado, N. Fujima, K. Harigaya, H. Shimizu, and A. Sakuma, *Phys. Rev. B* **73**, 172410 (2006).
- ¹³D. Gölden, E. Hildebrandt, and L. Alff, *J. Magn. Magn. Mater.* **422**, 407 (2017).
- ¹⁴W. B. Mi, Z. B. Guo, X. P. Feng, and H. L. Bai, *Acta Mater.* **61**, 6387 (2013).
- ¹⁵Y. Na, C. Wang, J. Xiang, N. Ji, and J. P. Wang, *J. Cryst. Growth* **426**, 117 (2015).
- ¹⁶H. Xiang, F. Y. Shi, M. S. Rzchowski, P. M. Voyles, and Y. A. Chang, *J. Appl. Phys.* **109**, 07E126 (2011).
- ¹⁷J. Li, Y. Jiang, T. Ma, C. Lu, Y. Xu, D. Yang, and M. Yan, *Physica B* **407**, 4783 (2012).
- ¹⁸K. Ito, K. Okamoto, K. Harada, T. Sanai, K. Toko, S. Ueda, Y. Imai, T. Okuda, K. Miyamoto, A. Kimura, and T. Suemasu, *J. Appl. Phys.* **112**, 013911 (2012).
- ¹⁹M. Tsunoda, Y. Komasaki, S. Kokado, S. Isogami, C. C. Chen, and M. Takahashi, *Appl. Phys. Express* **2**, 083001 (2009).
- ²⁰Y. Komasaki, M. Tsunoda, S. Isogami, and M. Takahashi, *J. Appl. Phys.* **105**, 07C928 (2009).
- ²¹L. Yin, W. Mi, and X. Wang, *Phys. Rev. Appl.* **6**, 064022 (2016).
- ²²L. Yin, X. Wang, and W. Mi, *Appl. Phys. Lett.* **111**, 032404 (2017).
- ²³Z. R. Li, X. P. Feng, X. C. Wang, and W. B. Mi, *Mater. Res. Bull.* **65**, 175 (2015).
- ²⁴K. Kabara, M. Tsunoda, and S. Kokado, *AIP Adv.* **6**, 055801 (2016).
- ²⁵S. F. Matar, A. Houari, and M. A. Belkhir, *Phys. Rev. B* **75**, 245109 (2007).
- ²⁶F. Takata, K. Kabara, K. Ito, M. Tsunoda, and T. Suemasu, *J. Appl. Phys.* **121**, 023903 (2017).
- ²⁷Y. Imai, Y. Takahashi, and T. Kumagai, *J. Magn. Magn. Mater.* **322**, 2665 (2010).
- ²⁸S. Kämmerer, A. Thomas, A. Hütten, and G. Reiss, *Appl. Phys. Lett.* **85**, 79 (2004).
- ²⁹Y. Sakuraba, J. Nakata, M. Oogane, H. Kubota, Y. Ando, A. Sakuma, and T. Miyazaki, *Jpn. J. Appl. Phys.* **44**(Part 2), L1100 (2005).
- ³⁰T. Ishikawa, T. Marukame, K. I. Matsuda, T. Uemura, M. Arita, and M. Yamamoto, *J. Appl. Phys.* **99**, 08J110 (2006).
- ³¹K. Moges, Y. Honda, H. Liu, T. Uemura, M. Yamamoto, Y. Miura, and M. Shirai, *Phys. Rev. B* **93**, 134403 (2016).
- ³²M. S. Gabor, M. Belmehenni, T. Petrisor, C. Ulhaq-Bouillet, S. Colis, and C. Tiusan, *Phys. Rev. B* **92**, 054433 (2015).
- ³³L. L. Wang, W. T. Zheng, J. Gong, H. B. Li, X. Wang, N. Ma, P. J. Cao, and X. C. Ma, *J. Alloys Compd.* **467**, 1 (2009).
- ³⁴A. Narahara, K. Ito, T. Suemasu, Y. K. Takahashi, A. Ranajikanth, and K. Hono, *Appl. Phys. Lett.* **94**, 202502 (2009).
- ³⁵S. X. Huang, T. Y. Chen, and C. L. Chien, *Appl. Phys. Lett.* **92**, 242509 (2008).
- ³⁶J. R. Shi and J. P. Wang, *Thin Solid Films* **420–421**, 172 (2002).
- ³⁷N. Ji, M. S. Osofsky, V. Lauter, L. F. Allard, X. Li, K. L. Jensen, H. Ambaye, E. Lara-Curzio, and J. P. Wang, *Phys. Rev. B* **84**, 245310 (2011).
- ³⁸X. Li, H. Li, M. Jamali, and J. P. Wang, *AIP Adv.* **7**, 125303 (2017).
- ³⁹Y. Qi, X. Liu, W. Huang, H. Lu, and J. Gao, *Vacuum* **133**, 13 (2016).
- ⁴⁰R. Desai, V. Davariya, K. Parekh, and R. V. Upadhyay, *Pramana: J. Phys.* **73**, 765 (2009).
- ⁴¹V. Ng, J. F. Hu, A. O. Adeyeye, J. P. Wang, and T. C. Chong, *J. Appl. Phys.* **91**, 7206 (2002).
- ⁴²S. Upadhyay, A. Palanisami, R. Louie, and R. Buhrman, *Phys. Rev. Lett.* **81**, 3247 (1998).
- ⁴³T. Y. Chen, S. X. Huang, and C. L. Chien, *Phys. Rev. B* **81**, 214444 (2010).
- ⁴⁴X. Li, M. S. Osofsky, K. L. Jensen, H. Li, and J. P. Wang, *AIP Adv.* **7**, 095001 (2017).
- ⁴⁵S. Matar, P. Mohn, G. Demazeau, and B. Siberchicot, *J. Phys. Fr.* **49**, 1761 (1988).
- ⁴⁶A. Sakuma, *J. Magn. Magn. Mater.* **102**, 127 (1991).
- ⁴⁷Y. J. Shi, Y. L. Du, and G. Chen, *Solid State Commun.* **152**, 1581 (2012).
- ⁴⁸R. Masrour, A. Jabar, and E. K. Hllil, *J. Magn. Magn. Mater.* **453**, 220 (2018).